

Study on Aerodynamic Flow Characteristics of the Box Girders by Different Turbulence Models

Ilker Goktepe^{*}

Department of Mechanical Engineering, Konya Technical University, Konya, Türkiye

Received 6 May 2024; Accepted 3 December 2024

Abstract

The aim of the study is to examine aerodynamic flow characteristics of a box girder and a twin-box girder have been investigated at $Re = 20000$. The methods based on $k-\epsilon$ and $k-\omega$ turbulence models have been compared. The minimum pressure has been observed on the lower surfaces for the box girder. Nevertheless, it has been provided for the upper surfaces of the twin-box girder. The highest value for turbulent kinetic energy has been obtained below the downstream fairing of the box girder. The same value has been attained in the slot. Lower values are weaker for the streamwise velocity components of the box girder. The lowest values have been seen in the gap of the twin-box girders and it behaved like a cavity. For cross-stream velocity components, maximum and minimum values depended on the rotational direction of the clusters. The wake has been enlarged perpendicular to flow for the twin-box girder, however, the wake shrunk due to the same effect. For the wake region, turbulence model and girder type have strongly influenced the velocity magnitude profiles. Drag coefficients are in good agreement with those previously reported. However, $k-\omega$ SST turbulence model has been suggested by a little margin.

Keywords: Box girder, drag coefficient, Reynolds number, turbulence model, twin-box girder

1. Introduction

Wind characteristics are considered for bridge design. For long-span bridges, aerodynamic performance is a significant case [1]. Because these bridges have higher flexibility and lower capability for damping [2]. Therefore, a streamlined box girder is utilized to improve the wind resistance. Moreover, a twin-box girder is another bridge structure for the possible application. When the previous studies are examined, the following ones are listed. Shirai and Ueda [3] conducted numerical simulations for the aerodynamics characteristics of a flat box girder. Ma et al. [4] applied active control for flow approaching to a streamlined box girder for the wind tunnel experiments. Li et al. [5] considered the flow characteristics around a twin-box girder in terms of various Reynolds number values of the experimental study. Laima and Li [2] scrutinized the effects of gap width and vortex-induced vibration on flow around twin-box girders for the experimental study. Trein et al. [6] experimentally studied the pressure characteristics of box girders by considering the gap effect. Yang et al. [7] presented an experimental study for the examination of flow around twin-box girder bridges with several slot widths. Laima et al. [8] examined the effect of Reynolds number flow structures around a twin-box girder by using Large Eddy Simulation (LES) turbulence model. Similarly, the effects of attachments on flow structures of a twin-box girder have also been studied by Laima et al. [9]. Chen et al. [10] conducted experiments for the application of passive flow control on a single box girder at $Re = 28000$. Ma et al. [11] considered the wind field characteristics acting on a twin-box girder of the experimental study. Noguchi et al. [12] implemented LES turbulence model to examine the influence of the forced oscillation method on the aerodynamic

characteristics of a box girder bridge for $Re = 2000$ and $Re = 20000$. He et al. [13] conducted LES simulations to investigate the flow around parallel box girders in terms of different gap-width ratios. Li et al. [1] presented a study including both experimental and numerical techniques for the investigation of flow characteristics of a streamlined box girder at $Re = 16000$. The effect of attack angle has been considered in their study for the range of $-12^\circ \leq \alpha \leq 12^\circ$. Fan et al. [14] positioned two box girders in parallel configuration in terms of a numerical study. Yan et al. [15] studied the vortex-induced vibration of a box girder. Zhang et al. [16] used LES turbulence model for flow around a flat box girder at $Re = 40000$. Haldar and Karmakar [17] prepared a parametric study covering flow characteristics of a box girder bridge. Single and double decks subjected to varying attack angle values have been utilized. Wang et al. [18] numerically investigated the vortex-induced vibration for a streamlined box girder having barriers filled by water. Wu et al. [19] considered a double-slotted box girder for both experimental and numerical methods. Meng et al. [20] used a triple-box girder for the investigation of flow characteristics in terms of varying Reynolds numbers.

The motivation of the study is to investigate the aerodynamic performance of the box-girders by using different turbulence models. As is well-known, the experimental systems might not be available for the design process of long-span bridges. Thus, Computational Fluid Dynamics (CFD) is a stronger method for the comparison of aerodynamic stability of the box girders. However, turbulent flow characteristics are very dominant around the box girders. For this reason, the determination of the appropriate turbulence model is a key step for the design stage. In terms of the present problem, wind flow characteristics and drag coefficient have been obtained by several turbulence models. The comparison for these methods has also been made for the

^{*}E-mail address: igoktepe@ktun.edu.tr

ISSN: 1791-2377 © 2024 School of Science, DUTH. All rights reserved.

doi:10.25103/jestr.176.10

examination of aerodynamic properties of different box girders.

2. Method

Various turbulence models have been compared for the case of flow around the box girders. Air flow characteristics of a box girder and a twin-box girder have been numerically examined by implementing the turbulence models of k-ε Realizable, k-ε Renormalization Group (RNG), Standard k-ω and k-ω Shear Stress Transport (SST). The turbulence models have been chosen due to their wide-spread utilization for flows including rotation and separation.

Considering the study having both experimental and numerical parts by Li et al. [1], the height for a box girder has been taken as $D = 30$ mm and its width was $9.333D$ in terms of comparison as in Fig. 1. Moreover, a twin-box has also been used. The only difference between the box girder and the twin-box girder is the central slot with the width of $1.556D$. For comparison, the slot width has been determined by taking the studies [8, 9] into account. The ratio of the slot width to the box girder width is approximately 0.167 in these studies. The flow domains have been established as two-dimensional and their dimensions are similar to ones as in the study by Li et al. [1]. Regarding the reference study, the dimensions are $-93.333 \leq x^* = x/D \leq 186.667$ in streamwise direction and $-93.333 \leq y^* = y/D \leq 93.333$ in cross-stream direction. However, Reynolds number of $Re = 20000$ has been taken into account for the comparison of different turbulence models. For the calculation of Reynolds number, $Re_D = U_\infty D/\nu$ has been used. For this equation, the values for $U_\infty = 9.74$ m/s and $D = 0.03$ m have been considered with the kinematic viscosity of air.

At the inlet, uniform velocity has been defined. For the exit, pressure outlet has been used since the gauge pressure is valid due to atmospheric conditions. No-slip boundary condition has been implemented for the box girder. The rest of the flow domain has symmetric boundary condition.

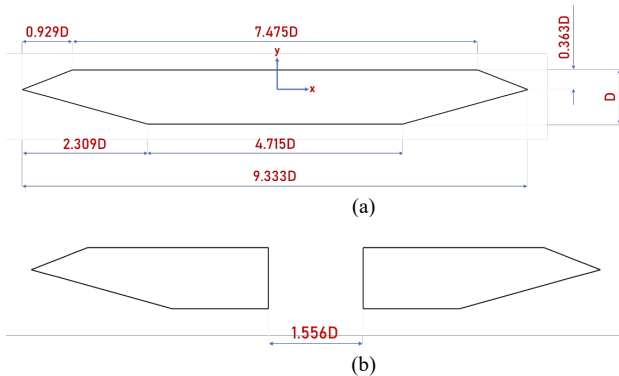


Fig. 1. Schematic views for (a) the box girder and (b) the twin-box girder

For the turbulence modeling, related equations have been used by the commercial numerical solver. The equations for continuity and momentum have been depicted in Eqs. 1 and 2 [21, 22]:

$$\frac{\partial \rho}{\partial t} + \frac{\partial}{\partial x_i}(\rho u_i) = 0 \quad (1)$$

$$\frac{\partial}{\partial t}(\rho u_i) + \frac{\partial}{\partial x_i}(\rho u_i u_j) = -\frac{\partial \rho}{\partial x_i} + \frac{\partial}{\partial x_j} \left[\mu \left(\frac{\partial u_i}{\partial x_j} + \frac{\partial u_j}{\partial x_i} - \frac{2}{3} \delta_{ij} \frac{\partial u_l}{\partial x_l} \right) \right] + \frac{\partial}{\partial x_j}(-\rho \overline{x'_i x'_j}) \quad (2)$$

Less computational capacity is required for average properties considered in terms of the present case. Regarding this explanation, k-ε and k-ω based turbulence models have been utilized.

Realizable module is a modified one when compared to other ones. The current model is used to model boundary-free shear and rotational flows. Turbulent kinetic energy is k and its dissipation rate is shown by ε as in Eqs. 3 and 4 [21, 22]:

$$\frac{\partial}{\partial t}(\rho k) + \frac{\partial}{\partial x_i}(\rho k u_i) = \frac{\partial}{\partial x_j} \left[\mu \frac{\partial k}{\partial x_j} \right] + G_k - \rho \varepsilon + S_k \quad (3)$$

$$\frac{\partial}{\partial t}(\rho \varepsilon) + \frac{\partial}{\partial x_i}(\rho \varepsilon u_i) = \frac{\partial}{\partial x_j} \left[\mu \frac{\partial \varepsilon}{\partial x_j} \right] + \rho C_1 S_\varepsilon - \rho C_2 \frac{\varepsilon^2}{k + \sqrt{\nu \varepsilon}} + S_\varepsilon \quad (4)$$

Production of turbulent kinetic energy stands for G_k because of mean velocity gradients. The source terms are S_k and S_ε [21-23].

RNG module of k-ε turbulence model is based on analytical derivation with the constants, the additional terms and the equations for the transport functions with respect to those used for standard k-ε model as in Eqs. 5 and 6 [21].

$$\frac{\partial}{\partial t}(\rho k) + \frac{\partial}{\partial x_i}(\rho k u_i) = \frac{\partial}{\partial x_j} \left[\mu_{eff} \alpha_k \frac{\partial k}{\partial x_j} \right] + G_k - \rho \varepsilon + S_k \quad (5)$$

$$\frac{\partial}{\partial t}(\rho \varepsilon) + \frac{\partial}{\partial x_i}(\rho \varepsilon u_i) = \frac{\partial}{\partial x_j} \left[\mu_{eff} \alpha_k \frac{\partial \varepsilon}{\partial x_j} \right] + C_{1\varepsilon} G_k \frac{\varepsilon}{k} - C_{2\varepsilon} \rho \frac{\varepsilon^2}{k} - R_\varepsilon + S_\varepsilon \quad (6)$$

The present model includes the refinement of its standard one. Furthermore, it is more sensitive in the estimation of the rapid strain and streamlines curvature effects [21].

Standard k-ω turbulence model is related to the method presented by Wilcox [24]. The model is very successful for the modeling of free shear flows and wall-bounded flows. The related equations are as in Eqs. 9 and 10.

$$\frac{\partial}{\partial t}(\rho k) + \frac{\partial}{\partial x_i}(\rho k u_i) = \frac{\partial}{\partial x_j} \left[\Gamma_k \frac{\partial k}{\partial x_j} \right] + G_k - Y_k + S_k \quad (7)$$

$$\frac{\partial}{\partial t}(\rho \omega) + \frac{\partial}{\partial x_i}(\rho \omega u_i) = \frac{\partial}{\partial x_j} \left[\Gamma_\omega \frac{\partial \omega}{\partial x_j} \right] + G_\omega - Y_\omega + S_\omega \quad (8)$$

Production of turbulent kinetic energy is indicated by G_k and G_ω is valid for the production of ω . The effective diffusivity terms are Γ_k and Γ_ω for k and ω , respectively. For k and ω , the dissipation terms are defined by Y_k and Y_ω , respectively. The derivations are the user-defined ones for S_k and S_ω [21-23].

In the problems including fluid-structure interaction, free shear layer, reverse pressure gradient, k-ω SST turbulence model is widely preferred as a variation of its standard method. The replacement for turbulent viscosity due to the turbulent shear stress transport. Mixing function and cross-diffusion for ω and are necessitated. Then, the turbulence model becomes more efficient around near wall and far field sections. The transport equations for k-ω SST turbulence model have been given as stated in Eqs. 9 and 10 [21-23]:

$$\frac{\partial}{\partial t}(\rho k) + \frac{\partial}{\partial x_i}(\rho k u_i) = \frac{\partial}{\partial x_j} \left[\Gamma_k \frac{\partial k}{\partial x_j} \right] + G_k - Y_k + S_k \quad (9)$$

$$\frac{\partial}{\partial t}(\rho \omega) + \frac{\partial}{\partial x_i}(\rho \omega u_i) = \frac{\partial}{\partial x_j} \left[\Gamma_\omega \frac{\partial \omega}{\partial x_j} \right] + G_\omega + D_\omega - Y_\omega + S_\omega \quad (10)$$

Production of turbulent kinetic energy is G_k and G_ω is used to produce ω . The effective diffusivity terms for k and ω are Γ_k and Γ_ω , respectively. Dissipation terms for k and ω are identified as Y_k and Y_ω , respectively. The cross-diffusion term is also D_ω and the derivations for S_k and S_ω are the user-defined ones [21-23].

The grid structures having 440 000, 570 000, 780 000 and 960 000 have been compared for drag coefficients obtained by several turbulence models. The results have been given in Fig. 2. These results are in good agreement with the ranges presented by Li et al. [1].

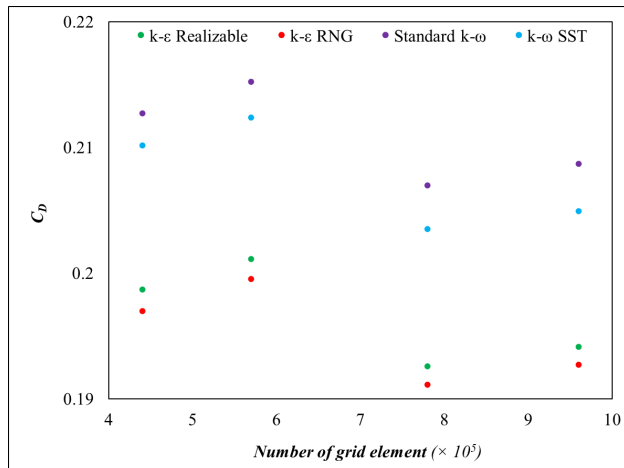


Fig. 2. Comparison of drag coefficients obtained by the turbulence models for different grid structures

With respect to the results of the grid independence test, drag coefficients attained by the grid numbers of 780 000 and 960 000 are very close. Therefore, the grid number of 780 000 has been chosen as more appropriate for the numerical simulations. The convergence has been observed by the criterion of 10^{-6} for continuity, momentum and turbulence model equations.

3. Results and Discussion

The study by Li et al. [1] is a reference one to compare the several turbulence models. Flow characteristics around the box girders have been numerically investigated at $Re = 20000$ for the design of the wind-resistant bridges. For this reason, a streamlined box girder and a twin-box girder have been used for numerical simulations to evaluate the aerodynamic stability including flow patterns and drag coefficients. All values have been presented as dimensionless. The legend bar has been kept constant for the contour graphics given for the same one.

In terms of pressure distributions, the results have been given in upstream and downstream regions for $-10 \leq x^* \leq 33.83$ in the flow direction and $-20 \leq y^* \leq 20$ in the cross-stream direction. In terms of $P^* = P \rho^{-1} U_\infty^{-2}$, the maximum value is $P^*_{max} = 0.3$, however, the minimum value is $P^*_{min} = -0.2$ as in the legend consisting of fifteen divisions for Fig. 3. The peak value for pressure has been attained at the contact point for flow and the body. This point indicated flow stagnation around the upstream fairing. Owing to the flow

separation, the lower value for pressure has been observed on the lower surfaces for the box girder. Nonetheless, this value has been provided for the upper surfaces of the upstream one in case of the twin-box girder. Furthermore, there are values close to the maximum ones around the downstream fairings. However, this effect has relatively disappeared by the slots of the twin-box girders. Separated flow triggered lower pressure region. The numerical results of k-ε and k-ω based turbulence models are similar. The average pressure values are more effective for the cases of the same turbulence models.

Turbulent kinetic energy values have been presented for $-10 \leq x^* \leq 33.83$ in the streamwise direction and $-20 \leq y^* \leq 20$ in the cross-stream direction. For $TKE^* = TKE U_\infty^{-2}$, the peak value is $TKE^*_{max} = 0.01$ and the lowest value is $TKE^*_{min} = 0$ for the legend with fifteen divisions in Fig. 4. The highest value has been obtained below the downstream fairing of the box girder. Nevertheless, the same value has been attained between the upstream and the downstream parts of the twin-box girder. What is more, two independent clusters have been seen. A larger cluster has been observed and its position was around the lower half of the slot. After the slot, the values tended to suddenly drop in the wake region. However, these values conserved its trend even in the wake region since there was no slot effect. The reason is the retardation of flow recovery. Owing to the turbulence generation by the flow separation, turbulence intensity increased for the related regions. It is because of local fluctuations in the zones.

Streamwise velocity components have been depicted as $u^* = u U_\infty^{-1}$. The maximum value is $u^*_{max} = 1.15$, however, the minimum value is $u^*_{min} = -0.05$ as shown by the legend having fifteen divisions. The values are valid for $-10 \leq x^* \leq 33.83$ in the streamwise direction and $-20 \leq y^* \leq 20$ in the cross-stream direction as in Fig. 5. The results of the turbulence models are nearly the same. However, the dominance of higher values is much more for the results of the twin-box girder. The maximum values have been observed around both upper and lower surfaces of the box girders. Lower values are weaker for the numerical values of the streamlined box girder. On the other hand, the lowest values have been seen between the upstream and the downstream parts of the twin-box girders. This section behaved like a cavity. Moreover, the length of wake region tended to increase due to twin-box girder effect. The reason is the retardation of flow recovery. Cross-stream velocity components have been presented in Fig. 6 for $v^* = v U_\infty^{-1}$. The highest value is $v^*_{max} = 0.22$ and the lowest one is $v^*_{min} = -0.22$ as in the legend including fifteen divisions. The values are in the ranges of $-10 \leq x^* \leq 33.83$ and $-20 \leq y^* \leq 20$. The results of the turbulence models are approximately similar. Nonetheless, the dominance of higher values is much more for the results of the streamlined box girder. The maximum values have been observed around lower surfaces of the streamlined box girder. The same situation is also valid for the minimum values in case of the streamlined one. It is related to the rotational direction of the clusters. For the twin-box girder, the highest value has been seen over the upstream fairing and the lowest one has been observed below the upstream fairing. However, the size of negative cluster is larger. The cavity flow has affected to enlarge negative cluster in the wake region. However, it triggered the shrinkage of positive cluster for the same zone.

Vorticity magnitude values have been given as $\omega^* = \omega D U_\infty^{-1}$ in Fig. 7. With respect to these graphics, the peak value is $\omega^*_{max} = 1$ and the minimum one is $\omega^*_{min} = 0$ as given in the legend covering fifteen divisions. The vorticity magnitude values have been presented in the ranges of $-10 \leq x^* \leq 33.83$ and $-20 \leq y^* \leq 20$ for the vorticity magnitude values. The

results obtained by four turbulence models indicated similarity for flow patterns. However, the position of maximum values changed with respect to the girder type. For the box girder, it is located around the downstream fairing. On the other hand, it is positioned between the upstream and the downstream parts of the twin-box girder. When it comes to

the wake region, flow patterns have also been varied by the girder type. In terms of y-direction, the wake size has been enlarged by the twin-box girder. However, the wake shrunk due to the same effect. The vice versa is valid for the case of the box girder.

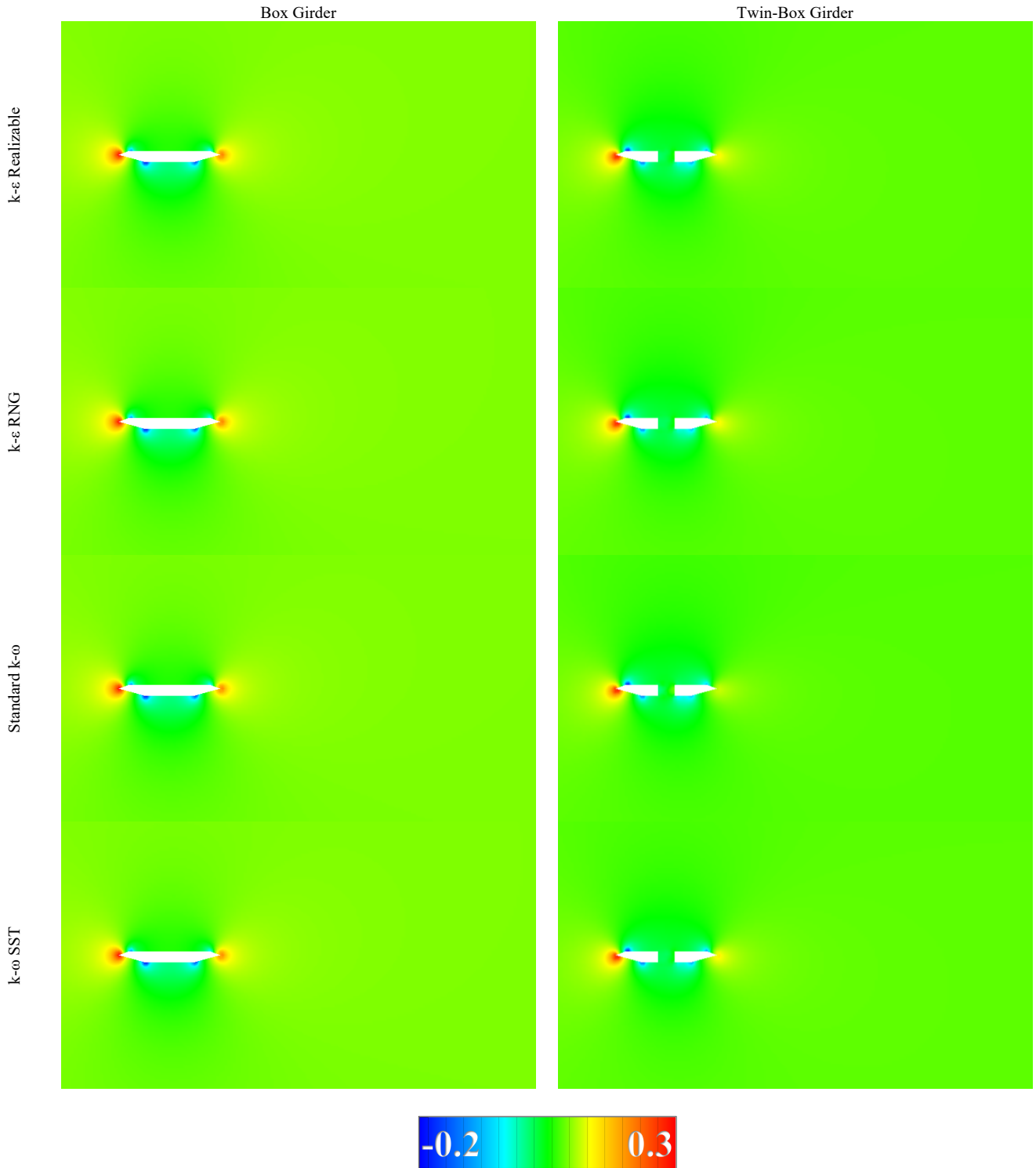


Fig. 3. Pressure distributions around the box girders

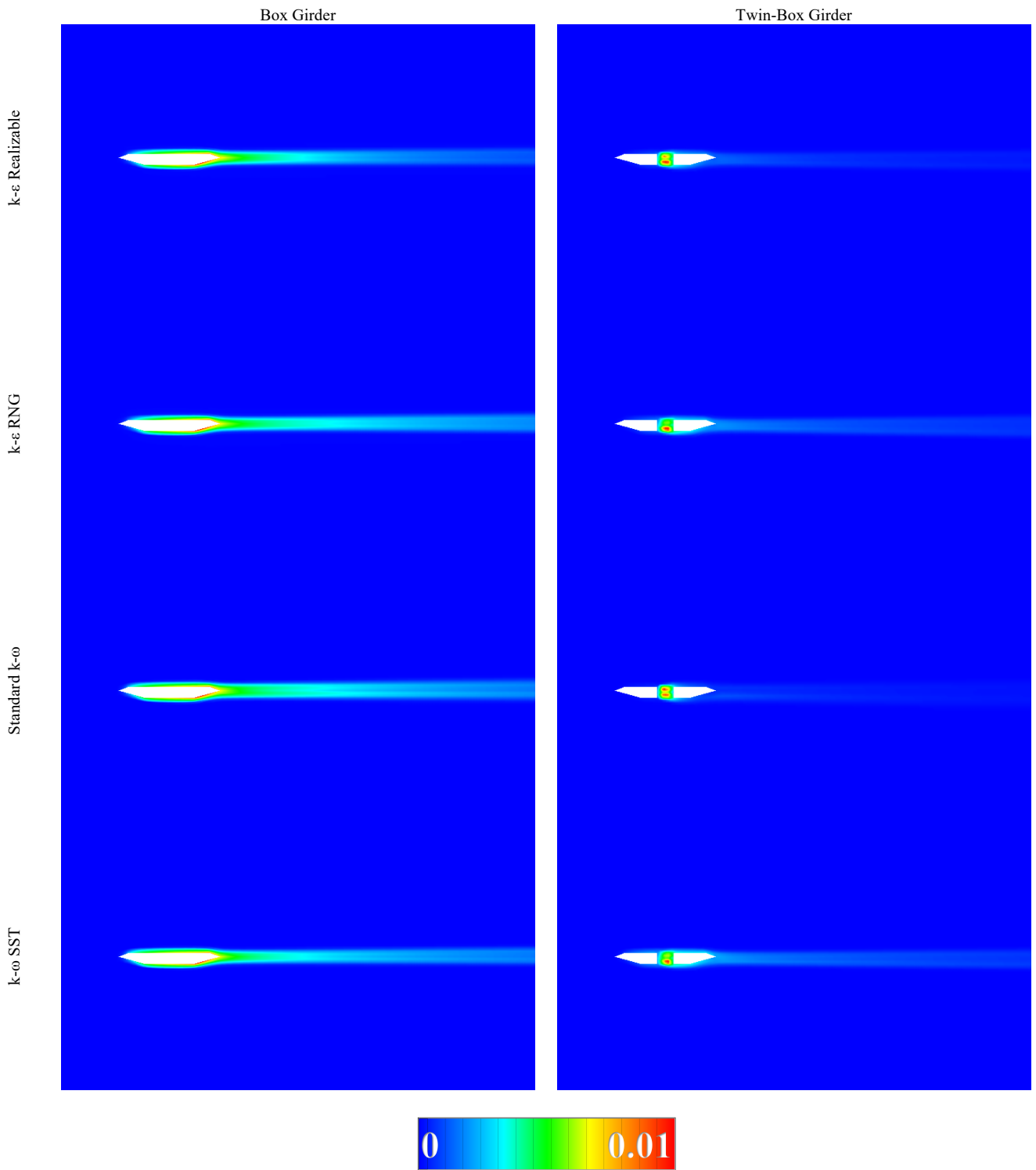
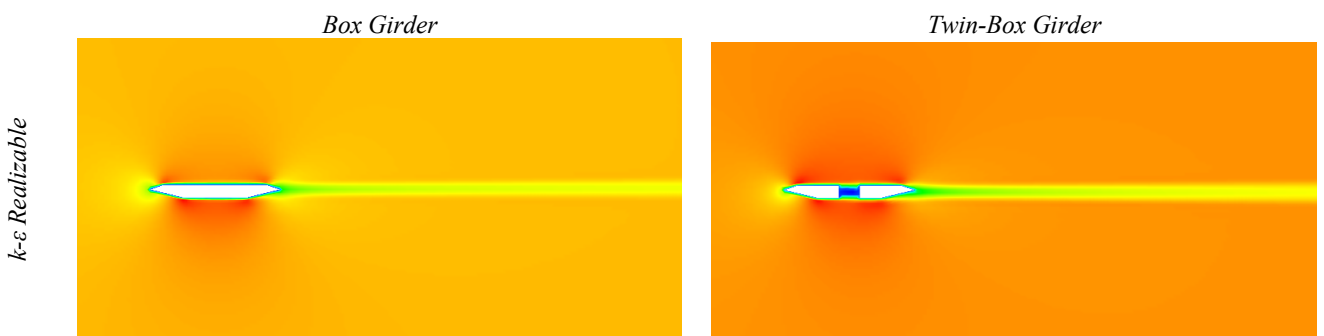


Fig. 4. Turbulent kinetic energy values around the box girders



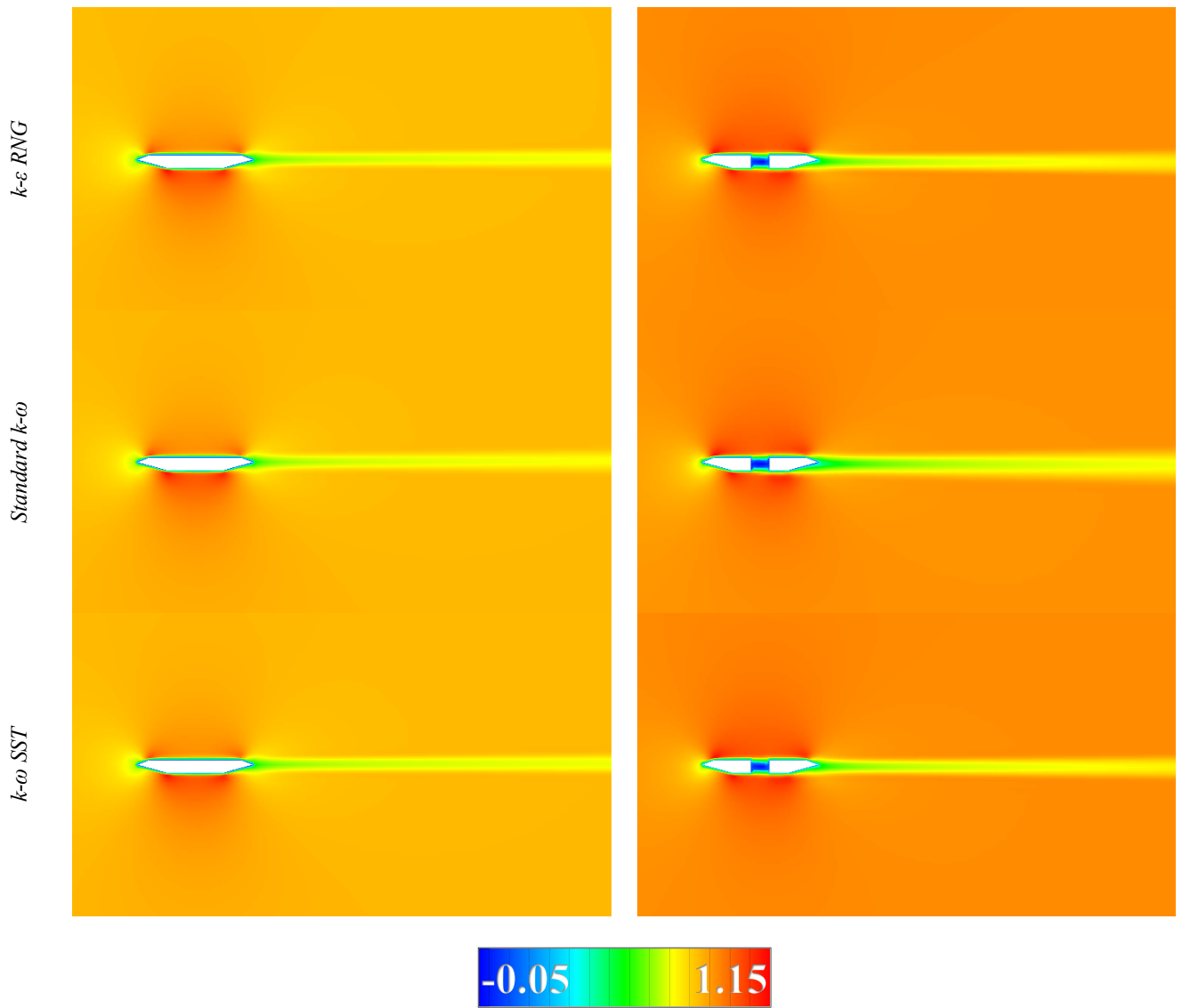
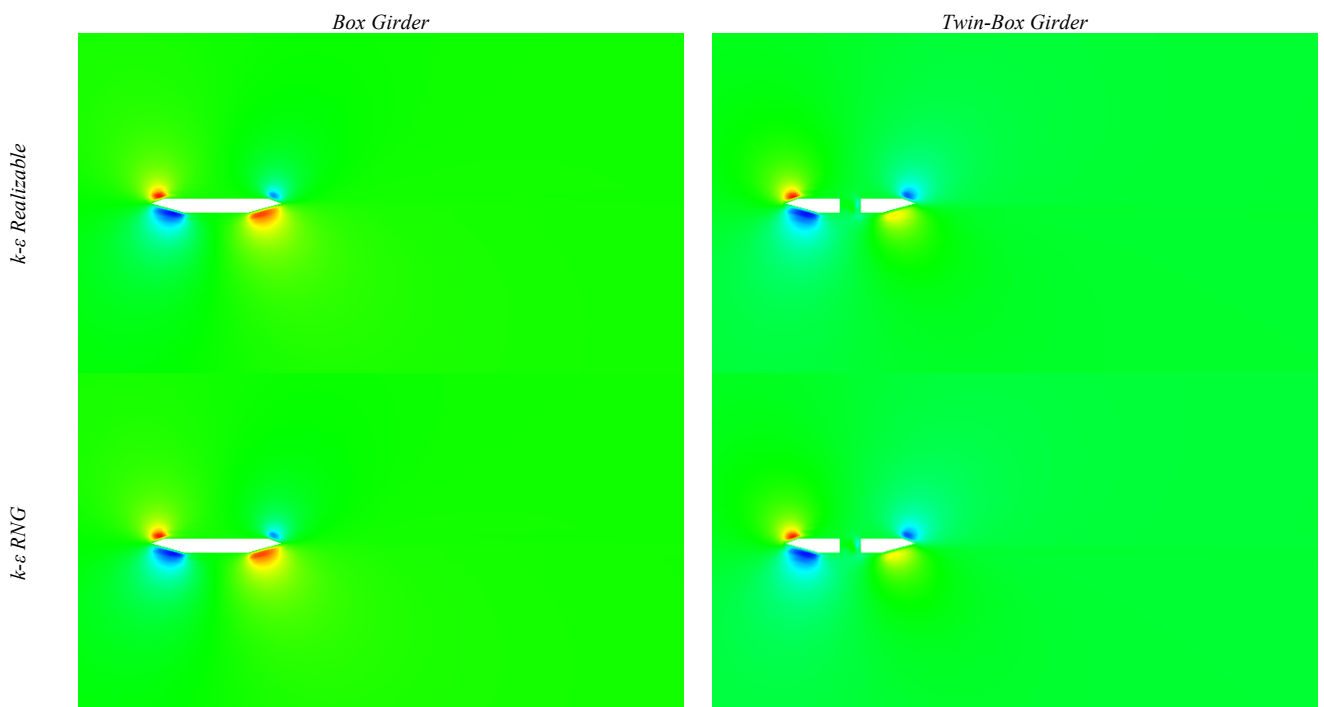


Fig. 5. Streamwise velocity components around the box girders



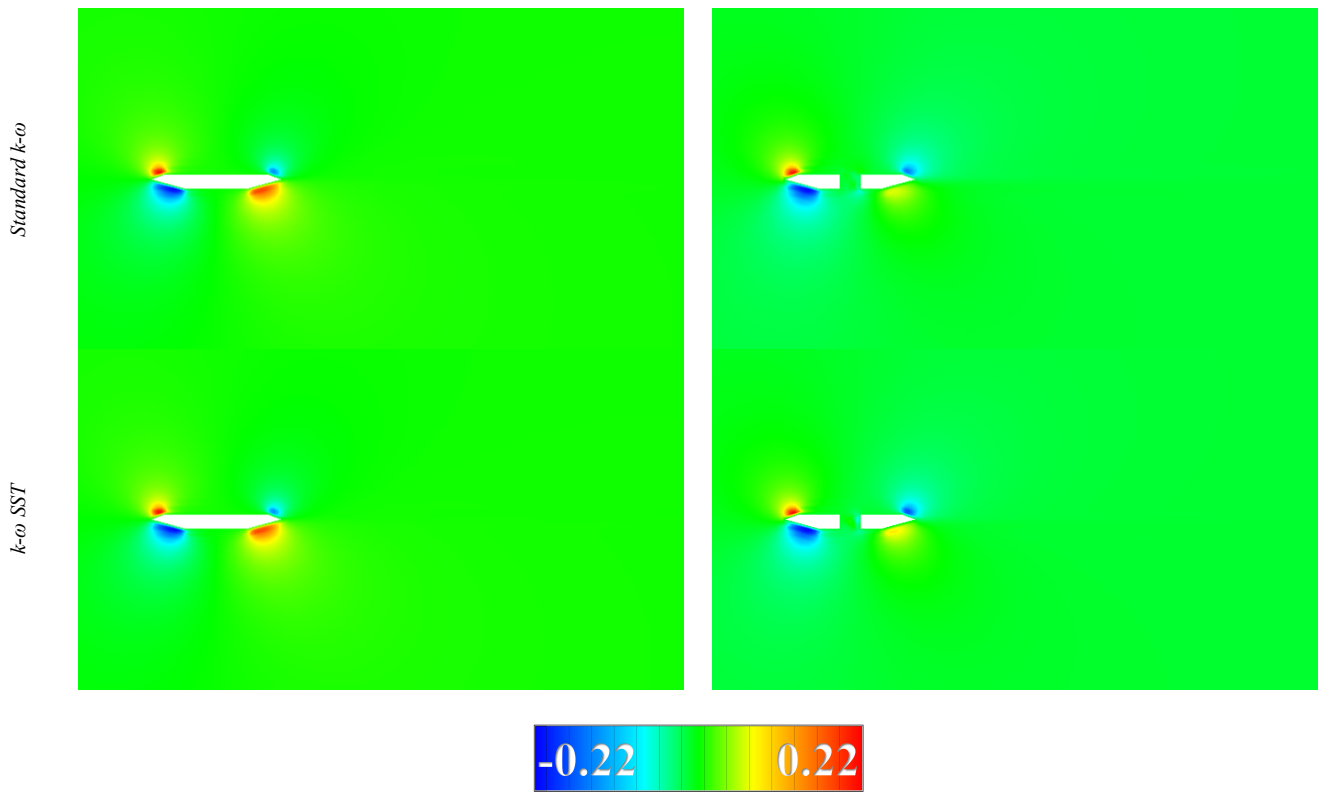
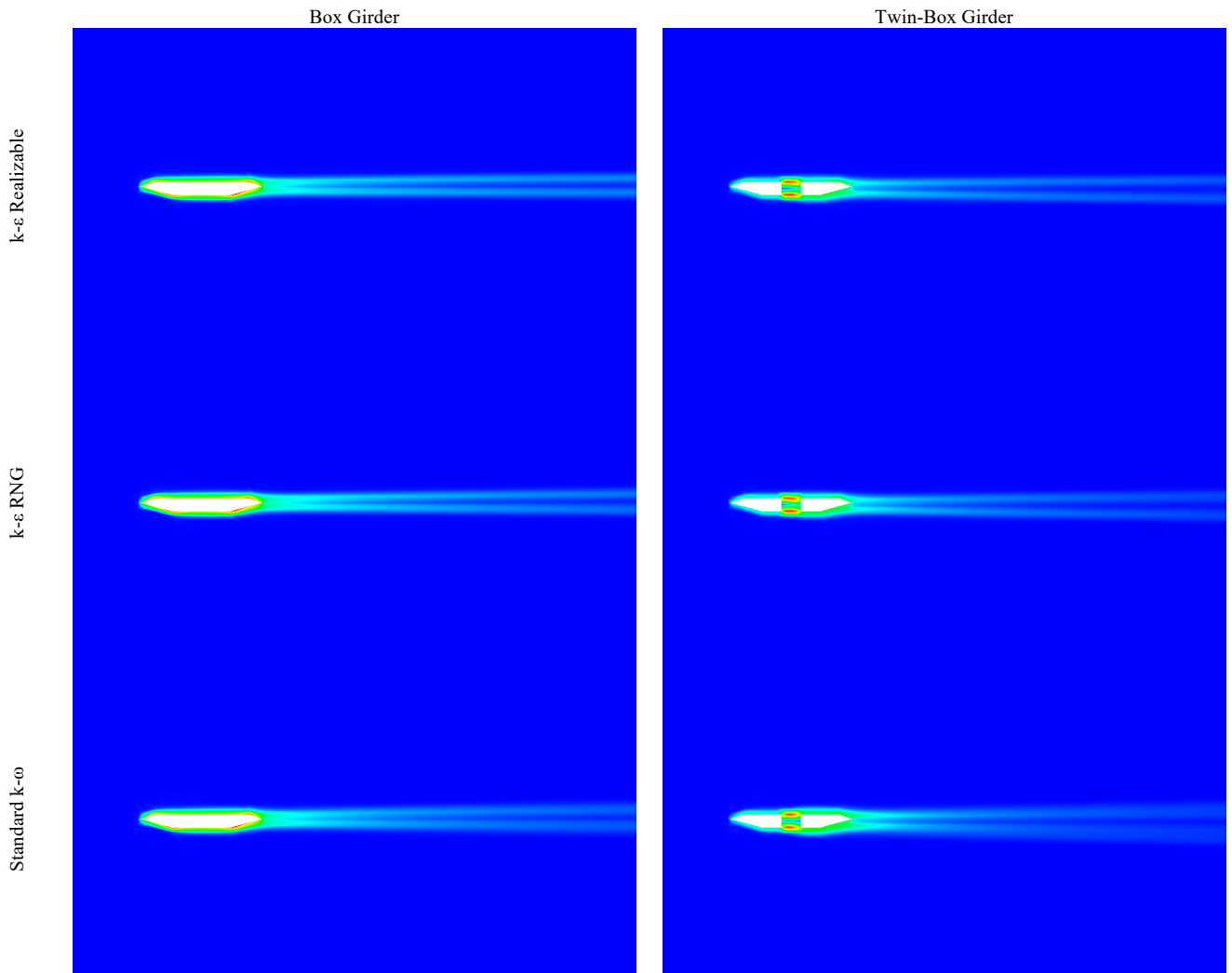


Fig. 6. Cross-stream velocity components around the box girders



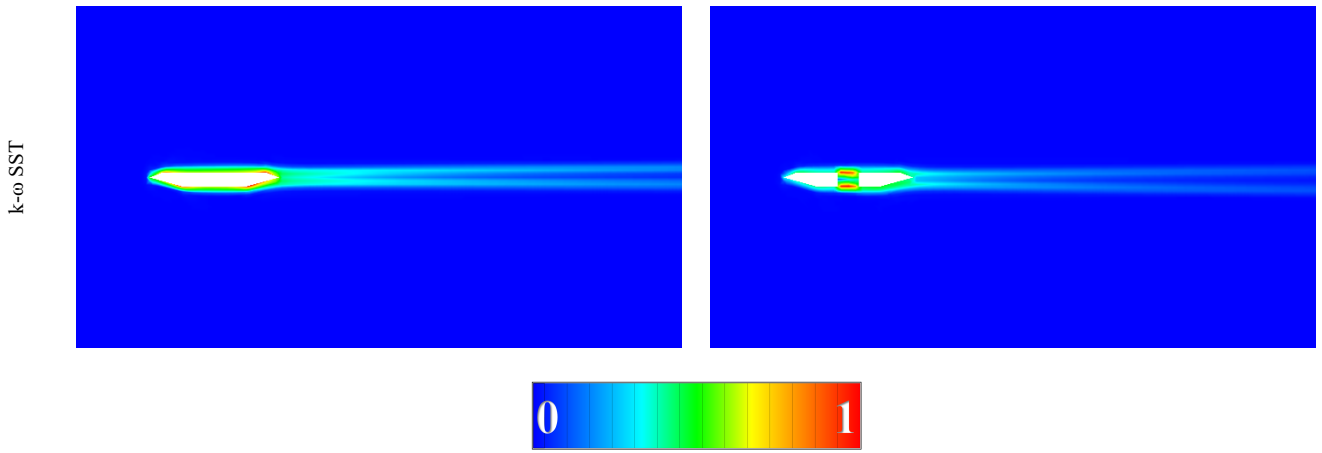


Fig. 7. Vorticity magnitude values around the box girders

The velocity magnitude profiles have been compared for different positions of Fig. 8 as $U^* = U U_\infty^{-1}$ depicted in Fig. 9. The box girder and the twin box girder have also been considered for this comparison. The streamwise positions have been ranged for $-6 \leq x^* \leq 8$. The positions have been chosen to indicate the effects of upstream, tip, fairing, corner, slot, downstream and far-wake at $x^* = -6$, $x^* = -4.67$, $x^* = -3.74$, $x^* = -2.36$, $x^* = 0$, $x^* = 2.36$, $x^* = 3.74$, $x^* = 4.67$, $x^* = 6$ and $x^* = 8$, respectively.

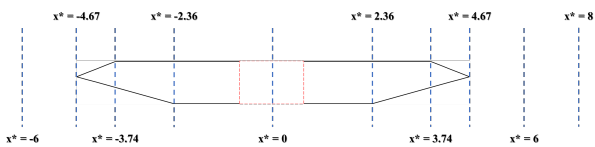
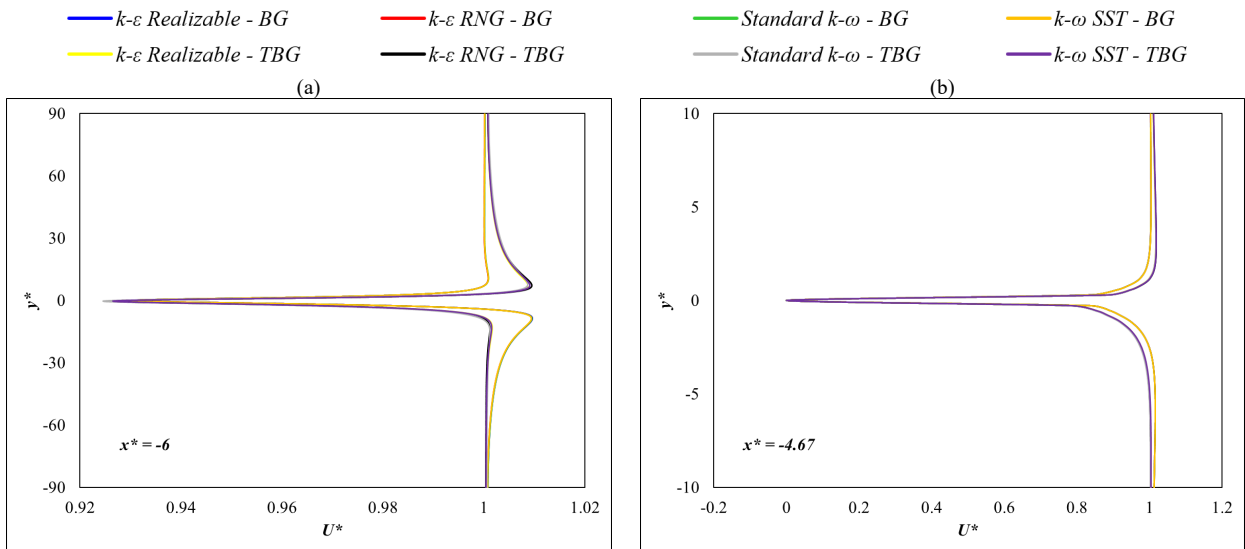


Fig. 8. Schematic representation of different positions for the box girder (BG) and the twin-box girder (TBG)

The velocity profiles differed by girder type effect. For $-4.67 \leq x^* \leq -2.36$, the change in velocity profile has only been observed by the design influence. For this reason, the results of turbulence models are nearly the same. Except for this range, the effects of turbulence models have been slightly seen in respect to velocity profiles. The girder type has also affected the upstream values. For the tip of the upstream fairing, there is considerable change with respect to $y^* = 0$. The effect of the twin-box girder is much more. In terms of $x^* = -3.74$ and $x^* = -2.36$, the value decrement and increment have been obtained for the box girder, respectively. Slot effect has been obviously attained for $x^* = 0$ as anticipated. For $x^* = 2.36$ and $x^* = 3.74$, the value increment and decrement have been obtained for the twin-box girder, respectively. For the wake region, both turbulence model and girder type have strongly affected the velocity magnitude profiles.



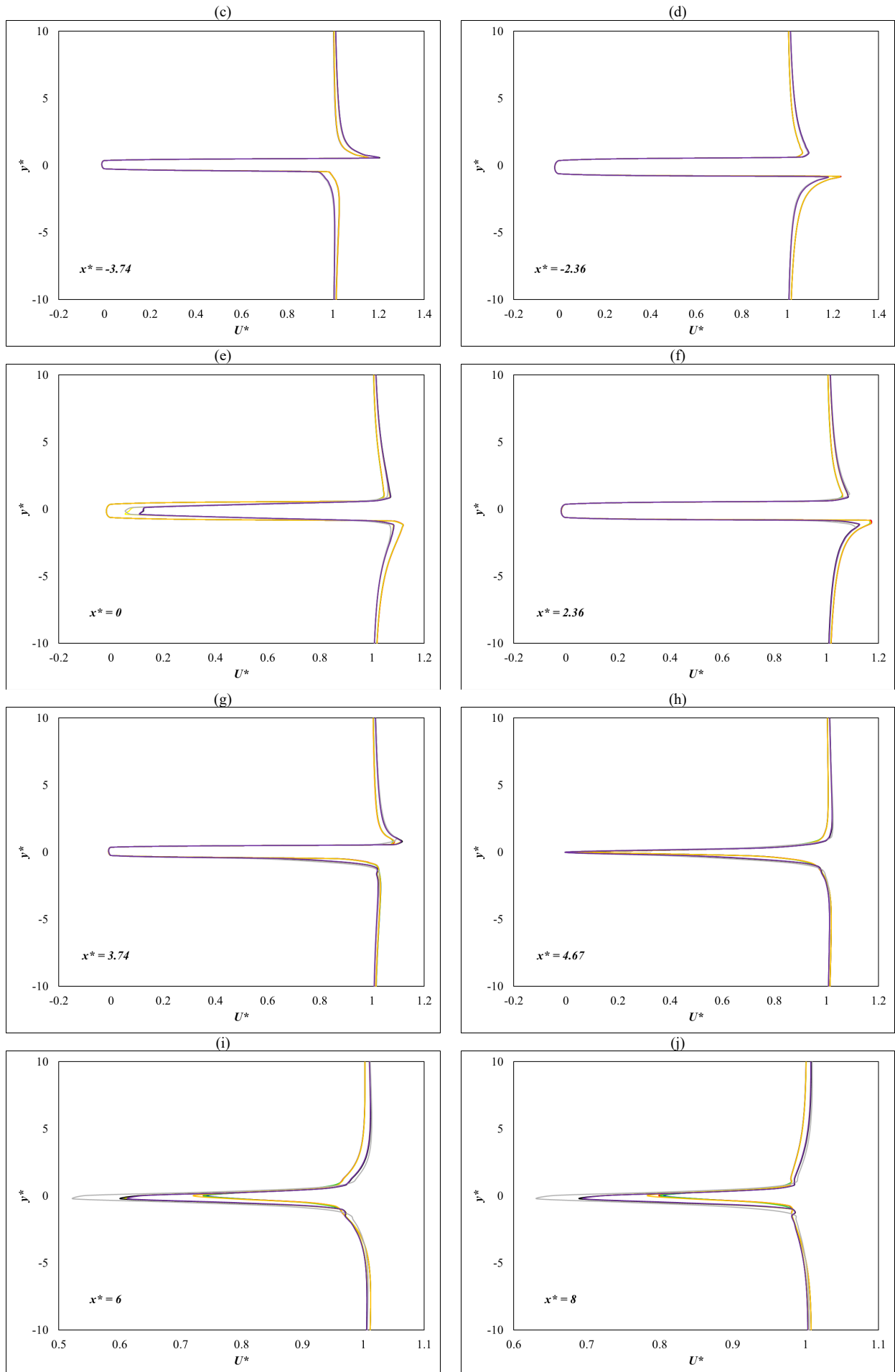


Fig. 9. Velocity magnitude profiles at various positions changing for flow direction

Drag coefficient for box girder and twin-box girder have been obtained by using various turbulence models. The numerical results have been presented for different conditions as in Table 1.

Table 1. Variation of drag coefficients obtained by turbulence models for girder type

Approach	Re	Girder Type	C _D
k-ε Realizable turbulence model	20000	Box girder	0.193
k-ε RNG turbulence model			0.191
Standard k-ω turbulence model			0.207
k-ω SST turbulence model			0.204
k-ε Realizable turbulence model			0.25 / 0.072
k-ε RNG turbulence model		Twin-box girder (Upstream / Downstream)	0.246 / 0.063
Standard k-ω turbulence model			0.287 / 0.164
k-ω SST turbulence model			0.245 / 0.056

The results are in good agreement with those reported in different studies [1, 2, 5]. Although the results of k-ε based turbulence models could be considered as acceptable, k-ω based turbulence models are more successful for this comparison. Among the k-ω based turbulence models, k-ω SST turbulence model has been recommended by a little margin.

4. Conclusions

A box girder and a twin-box girder have been compared in terms of flow characteristics obtained by using various turbulence models at Re = 20000. The numerical techniques

are k-ε Realizable, k-ε Renormalization Group (RNG), Standard k-ω and k-ω Shear Stress Transport (SST) turbulence models. These turbulence models have been tested for velocity profiles, drag coefficients and flow patterns including pressure distributions, turbulent kinetic energy values, streamwise velocity components, cross-stream velocity components and vorticity magnitude values. The minimum value for pressure has been obtained on the lower surfaces of the box girder. It has been observed for the upper surfaces of the twin-box girder. The peak value for turbulent kinetic energy has been attained below the downstream fairing for the box girder. The same value has been provided by the slot effect. For the streamwise velocity components of the box girder, lower values are weaker. In the case of the twin-box girders, the minimum values have been observed in the gap behaving like a cavity. For cross-stream velocity components, the highest and the lowest values are based on the rotational direction of the clusters. In terms of the twin-box girder, the wake size has been enlarged perpendicular to flow direction. On the other hand, the wake shrinkage has been seen owing to the same effect. It is vice versa for the case of the box girder. For the wake structure, girder type and turbulence model have strongly influenced the velocity magnitude profiles. Drag coefficient values are in good agreement with those presented in previous studies. Moreover, k-ω based turbulence models are more successful; however, k-ω SST turbulence model has been suggested due to little margin.

For future studies, different designs for box girder could be considered in terms of flow characteristics. Although this study presents the results for the defined dimensions, the slot dimensions should be tested and optimized by experimental and numerical studies. Flow around triple box girder should be investigated as an alternative case.

This is an Open Access article distributed under the terms of the Creative Commons Attribution License.



References

[1] H.-H. Li, L.-L. Zhang, B. Wu, Z.-J. Ni, and Y. Yang, "Effects of the angle of attack on the aerodynamic characteristics of a streamlined box girder," *Adv. Struct. Eng.*, vol. 24, no. 10, pp. 2090–2104, Feb. 2021, doi: 10.1177/13694332211992490.

[2] S. Laima and H. Li, "Effects of gap width on flow motions around twin-box girders and vortex-induced vibrations," *J. Wind Eng. Ind. Aerodyn.*, vol. 139, pp. 37–49, Feb. 2015, doi: 10.1016/j.jweia.2015.01.009.

[3] S. Shirai and T. Ueda, "Aerodynamic simulation by CFD on flat box girder of super-long-span suspension bridge," *J. Wind Eng. Ind. Aerodyn.*, vol. 91, no. 1–2, pp. 279–290, Jan. 2003, doi: 10.1016/S0167-6105(02)00351-3.

[4] T. T. Ma, L. Zhao, S. Y. Cao, Y. J. Ge, and H. Miyagi, "Investigations of aerodynamic effects on streamlined box girder using two-dimensional actively-controlled oncoming flow," *J. Wind Eng. Ind. Aerodyn.*, vol. 122, pp. 118–129, Aug. 2013, doi: 10.1016/j.jweia.2013.07.011.

[5] H. Li, S. Laima, and H. Jing, "Reynolds number effects on aerodynamic characteristics and vortex-induced vibration of a twin-box girder," *J. Fluids Struct.*, vol. 50, pp. 358–375, Aug. 2014, doi: 10.1016/j.jfluidstructs.2014.06.027.

[6] C. A. Trein, H. Shirato, and M. Matsumoto, "On the effects of the gap on the unsteady pressure characteristics of two-box bridge girders," *Engin. Struct.*, vol. 82, pp. 121–133, Nov. 2014, doi: 10.1016/j.engstruct.2014.10.036.

[7] Y. Yang, R. Zhou, Y. Ge, and L. Zhang, "Experimental studies on VIV performance and countermeasures for twin-box girder bridges with various slot width ratios," *J. Fluids Struct.*, vol. 66, pp. 476–489, Sep. 2016, doi: 10.1016/j.jfluidstructs.2016.08.010.

[8] S. Laima, C. Jiang, H. Li, W. Chen, and J. Ou, "A numerical investigation of Reynolds number sensitivity of flow characteristics around a twin-box girder," *J. Wind Eng. Ind. Aerodyn.*, vol. 172, pp. 298–316, Nov. 2017, doi: 10.1016/j.jweia.2017.11.016.

[9] S. Laima, H. Li, W. Chen, and J. Ou, "Effects of attachments on aerodynamic characteristics and vortex-induced vibration of twin-box girder," *J. Fluids Struct.*, vol. 77, pp. 115–133, Dec. 2017, doi: 10.1016/j.jfluidstructs.2017.12.005.

[10] G.-B. Chen, L.-Q. Zhang, W.-L. Chen, D.-L. Gao, W.-H. Yang, and H. Li, "Self-Suction-and-Jet control in flow regime and unsteady force for a single box girder," *J. Bridge Eng.*, vol. 24, no. 8, May 2019, doi: 10.1061/(asce)be.1943-5592.0001437.

[11] C. Ma, C. Pei, H.-L. Liao, M. Liu, and M. Li, "Field measurement and wind tunnel study of aerodynamic characteristics of twin-box girder," *J. Wind Eng. Ind. Aerodyn.*, vol. 202, May 2020, Art. no. 104209, doi: 10.1016/j.jweia.2020.104209.

[12] K. Noguchi, Y. Ito, and T. Yagi, "Numerical evaluation of vortex-induced vibration amplitude of a box girder bridge using forced oscillation method," *J. Wind Eng. Ind. Aerodyn.*, vol. 196, Nov. 2019, Art. no. 104029, doi: 10.1016/j.jweia.2019.104029.

- [13] X. He, X. Kang, L. Yan, R. G. J. Flay, P. Ren, and T. Wu, "Numerical investigation of flow structures and aerodynamic interference around stationary parallel box girders," *J. Wind Eng. Ind. Aerodyn.*, vol. 215, Jun. 2021, Art. no. 104610, doi: 10.1016/j.jweia.2021.104610.
- [14] S. Fan, W. Chen, H. Tang, and Y. Li, "Aerodynamic interference between two boxes in parallel arrangement and flow field characteristics around the girder," *Adv. Bridge Eng.*, vol. 3, no. 1, Dec. 2022, doi: 10.1186/s43251-022-00079-6.
- [15] Y. Yan, T. Yagi, K. Noguchi, Y. Ito, and R. Shimada, "Effects of handrail details on Vortex-Induced vibration for a Box-Girder bridge," *Bridge Eng.*, vol. 27, no. 3, Dec. 2021, doi: 10.1061/(asce)be.1943-5592.0001835.
- [16] Z. Zhang, F. Xu, X. Wang, and Y. Wang, "Instability modes of the flows around a streamlined box girder," *J. Wind Eng. Ind. Aerodyn.*, vol. 225, Apr. 2022, Art. no. 105008, doi: 10.1016/j.jweia.2022.105008.
- [17] P. Haldar and S. Karmakar, "Wind response on RC trapezoidal box girder bridge using computational fluid dynamics," *Sadhana*, vol. 48, no. 2, Apr. 2023, doi: 10.1007/s12046-023-02127-x.
- [18] X. Wang, F. Xu, Z. Zhang, Y. Wang, and M. Zhang, "Numerical explorations of the vortex-induced vibration of a streamlined box girder with water-filled barriers," *J. Wind Eng. Industr. Aerodyn.*, vol. 240, Jul. 2023, Art. no. 105496, doi: 10.1016/j.jweia.2023.105496.
- [19] F. Wu, Z. Wang, L. Zhao, T. Pan, H. Xiao, and Y. Ge, "Aerodynamic Force Distribution Characteristics around a Double-Slotted Box Girder of a Long-Span Bridge during Vortex-Induced Vibration," *J. Bridge Eng.*, vol. 28, no. 1, Nov. 2022, doi: 10.1061/(asce)be.1943-5592.0001977.
- [20] H. Meng, G. Chen, and D. Gao, "Aerodynamics and surrounding flow patterns of a long-span bridge girder model with triple-separated boxes," *Phys. Fluids*, vol. 36, no. 3, Mar. 2024, doi: 10.1063/5.0195734.
- [21] S. Yagmur, S. Dogan, M. H. Aksoy, and I. Goktepe, "Turbulence modeling approaches on unsteady flow structures around a semi-circular cylinder," *Ocean Eng.*, vol. 200, Feb. 2020, Art. no. 107051, doi: 10.1016/j.oceaneng.2020.107051.
- [22] I. Goktepe and U. Atmaca, "Examination of air flow characteristics over an open rectangular cavity between the plates," *Int. J. Aeroacoustics*, vol. 22, no. 3-4, pp. 351-370, Jun. 2023, doi: 10.1177/1475472x231185082.
- [23] I. Goktepe, U. Atmaca, and A. Cakan, "Investigation of Heat Transfer Augmentation between the Ribbed Plates via Taguchi Approach and Computational Fluid Dynamics," *J. Thermal Sci.*, vol. 29, no. 3, pp. 647-666, May 2019, doi: 10.1007/s11630-019-1155-z.
- [24] D. C. Wilcox, *Turbulence modeling for CFD*. 1993. [Online]. Available: <http://ci.nii.ac.jp/ncid/BA21991687>.